How slender can comb-drive fingers be?

2005 J. Micromech. Microeng. 15 1055

(http://iopscience.iop.org/0960-1317/15/5/023)

INSTITUTE OF PHYSICS PUBLISHING JOURNAL OF MICROMECHANICS AND MICROENGINEERING
J. Micromech. Microeng. **15** (2005) 1055–1059 doi:10.1088/0960-1317/15/5/023

How slender can comb-drive fingers be?

David Elata and Vitaly Leus

Faculty of Mechanical Engineering, Technion—Israel Institute of Technology, Haifa 32000, Israel

E-mail: elata@tx.technion.ac.il

Received 18 January 2005, in final form 1 March 2005
Published 8 April 2005
Online at stacks.iop.org/JMM/15/1055

Abstract
In this work, the electromechanical stability of individual comb-drive fingers is considered. Previous studies have shown that optimal design of elastic suspensions can prevent the side pull-in instability of comb-drive rotors. In this work it is shown that side pull-in can nevertheless occur in individual comb fingers, if they are exceedingly slender. To this end, the critical electromechanical state of individual comb fingers is analytically solved. This solution is in good agreement with finite elements simulations. The analytic solution can be used to design comb-drives in which side pull-in of individual fingers is avoided.

(Some figures in this article are in colour only in the electronic version)

1. Introduction

Electrostatic actuation is prevalent in MEMS devices due to its compatibility with microfabrication technology, ease of integration and low power consumption. Electrostatic actuation is achieved by applying a voltage difference between the electrodes of a deformable capacitor [1, 2]. In common electrostatic actuators one electrode is fixed and the other is connected to an elastic suspension. The electrostatic forces applied to the deformable electrode are balanced by the mechanical restoring forces that develop in the elastic suspension. To achieve considerable electrostatic forces without reverting to excessively high driving voltages the free-space gap between the electrodes must be minimal.

Electrostatic forces are inherently nonlinear and as a result the electromechanical response of electrostatic actuators may become unstable. The pull-in instability limits the stable travel range of the parallel-plates actuator to a third of the nominal gap [1, 2]. To enable large travel range while maintaining a minimal gap between the electrodes, comb-drive actuators were developed [3]. In comb-drive actuators the fixed electrode (stator) and mobile electrode (rotor) are each shaped as a comb with parallel rectangular fingers. The fingers of the stator and rotor combs are intertwined and are separated by a free-space gap (figure 1). The axial motion of the rotor is parallel to the fingers so that the gap is unaffected by the motion.

However, electromechanical instabilities may also occur in comb-drive actuators. The well-known side pull-in occurs in comb-drives when the electrostatic stiffness transverse to the axial direction of motion exceeds the transverse mechanical stiffness of the suspension [4, 5]. This side pull-in may be avoided by increasing the transverse stiffness of the suspension [6–8].

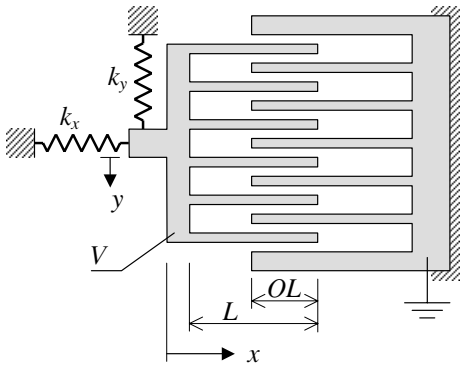

Figure 1. Schematic view of a single-sided comb-drive actuator with two degrees of freedom.

In previous studies of side pull-in in comb-drive actuators it was assumed that the rotor and stator are non-deformable rigid bodies. The side pull-in instability resulted from the transverse flexibility of the suspension that supports the rotor.

With the advancement of microfabrication technology, thinner fingers and smaller gaps can be micromachined. This can allow for a denser spacing of fingers and thus increase the power density of comb-drive actuators.

However, slender comb fingers cannot be considered as rigid, and side pull-in can develop due to the flexibility of

individual fingers. The purpose of this study is to analyze the stability of single fingers in comb-drives. Specifically, the parameters that dominate the side pull-in of individual fingers are derived. These parameters are important for proper design of comb-drive actuators.

2. Side pull-in of electrostatic comb-drives

In this section we revisit the problem of side pull-in of electrostatic comb-drives. A schematic view of a typical comb-drive actuator is shown in figure 1. The comb-drive is a deformable capacitor that is constructed from a stator and a rotor, each of which is made of many parallel fingers. The stator is mechanically fixed and the rotor is suspended on elastic springs. The elastic suspension is designed to enable the primary motion of the rotor in the x direction, parallel to the comb fingers. However, the suspension may also have some flexibility in the secondary transverse direction, y. For simplicity, it is assumed that the stiffness of the suspension is constant. The stator is grounded and the rotor is subjected to an electrostatic potential V. Due to the voltage difference, attractive electrostatic forces are induced between the stator and rotor. The electrostatic forces displace the rotor and give rise to mechanical restoring forces in the suspension. When the mechanical restoring forces balance the electrostatic driving forces, the actuator reaches an equilibrium state.

The electromechanical response of the comb-drive can be derived from the total potential given by

$$\psi = \frac{1}{2}k_x x^2 + \frac{1}{2}k_y y^2 - \frac{1}{2}N\varepsilon_0 b(OL + x) \times \left(\frac{1}{g-y} + \frac{1}{g+y}\right) V^2. \tag{1}$$

Here k_x and k_y are the stiffness coefficients of the two springs, N is the number of fingers in the rotor, ε_0 is the permittivity of free space, OL is the initial overlap between the rotor and stator, b is the depth of the fingers and g is the gap separating the stator and rotor fingers. The first two terms on the right-hand side of (1) are the elastic potential of the springs and the last term is the electrostatic complementary energy of the deformable capacitor (i.e. the electrostatic potential of the capacitor and the electrostatic potential of the voltage source).

The total potential may be rewritten in the following normalized form:

$$\tilde{\psi}(\tilde{x}, \tilde{y}, \tilde{V}) = \frac{1}{2}\tilde{x}^2 + \frac{1}{2}\tilde{k}\tilde{y}^2 - \frac{\tilde{O} + \tilde{x}}{1 - \tilde{y}^2}\tilde{V}^2 \tag{2}$$

where

$$\tilde{\psi} = \frac{\psi}{k_x L_e^2}, \qquad \tilde{k} = \frac{k_y g^2}{k_x L_e^2}, \qquad \tilde{V}^2 = \frac{N\varepsilon_0 b}{g k_x L_e} V^2$$
$$\tilde{x} = \frac{x}{L_e}, \qquad \tilde{y} = \frac{y}{g}, \qquad \tilde{O} = \frac{OL}{L_e} \tag{3}$$

and L_e is the expected travel range in the primary direction (e.g. $L_e < L - OL$).

The equilibrium states of the system are given by the partial derivative of the total potential with respect to the two degrees of freedom

$$\tilde{x} - \frac{1}{1 - \tilde{y}^2}\tilde{V}^2 = 0 \tag{4}$$

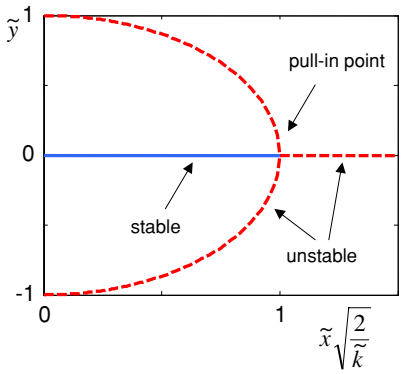

Figure 2. Equilibrium curves of the single-sided comb-drive actuator with two degrees of freedom (for $\tilde{O} = 0$).

$$\tilde{k}\tilde{y} - \frac{2(\tilde{O} + \tilde{x})\tilde{y}}{(1 - \tilde{y}^2)^2}\tilde{V}^2 = 0. \tag{5}$$

From equation (4) it is clear that as long as the symmetry in the transverse direction is maintained (i.e. $\tilde{y} = 0$), the primary motion is quadratically proportional to the control voltage $\tilde{V}$ applied to the rotor.

The equilibrium equations (4) and (5) have two possible solutions

$$\tilde{y} = 0; \qquad \tilde{x} = \tilde{V}^2 \tag{6}$$

and

$$\tilde{y} = \pm\sqrt{1 - (\tilde{O} + \tilde{x})2\tilde{x}/\tilde{k}}; \qquad 2\tilde{x}^2\frac{(\tilde{O} + \tilde{x})}{\tilde{k}} = \tilde{V}^2. \tag{7}$$

The solutions (6) and (7) are presented in figure 2 for the case of $\tilde{O} = 0$. In the first solution, the transverse displacement is identically zero (maintaining the transverse symmetry) and the primary displacement $\tilde{x}$ monotonically increases with applied voltage. The second solution describes two unstable equilibrium curves. These converging curves coincide, and intersect the first solution at the pull-in point. Up to this pull-in point the first solution is stable, and beyond this point it is unstable, as shown in figure 2. The stability of the equilibrium states can be determined by the determinant of the stiffness matrix [5]

$$K = \begin{pmatrix} \frac{\partial^2\tilde{\psi}}{\partial\tilde{x}^2} & \frac{\partial^2\tilde{\psi}}{\partial\tilde{x}\partial\tilde{y}} \\ \frac{\partial^2\tilde{\psi}}{\partial\tilde{x}\partial\tilde{y}} & \frac{\partial^2\tilde{\psi}}{\partial\tilde{y}^2} \end{pmatrix}. \tag{8}$$

At the pull-in point, where the two unstable solutions coincide, the term in the square root in (7) vanishes, yielding

$$\tilde{k} = 2(\tilde{x} + \tilde{O})\tilde{x}; \qquad \tilde{x} = \tilde{V}^2. \tag{9}$$

At this point, the actuator loses its stability in a bifurcation mode, and may collapse into contact with the stator in either transverse direction. This bifurcation loss of stability is the side pull-in [4].

A full travel range $\tilde{x} = 1$ is achieved by application of the voltage $\tilde{V}^2 = 1$, and side pull-in can be avoided within this travel range by satisfying $\tilde{k} > 2(1 + \tilde{O})$.

To enable large travel range of electrostatic comb-drives, folded-beam suspensions are used [3]. However, the transverse stiffness of folded-beam suspensions decreases with the increase of the primary displacement of the rotor [4].

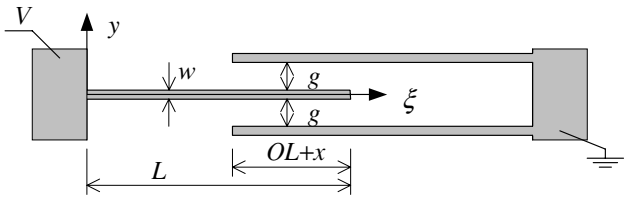

Figure 3. A single rotor finger between two stator fingers.

An elegant solution for this problem is using folded-beam suspensions with pre-curved beams [6–8]. The transverse stiffness of this suspension increases with the increase of the primary displacement. By using folded-beam suspensions with pre-curved beams, the rotor can be constrained to move only in the primary direction, and the side pull-in instability can practically be avoided.

In many MEMS devices, the suspension stiffness in the primary direction (k_x) is designed to ensure a minimal response time (i.e. natural frequency). Once this parameter has been set, in order to minimize the necessary driving voltages, the gap g should be minimized and the number of fingers N should be maximized (within the limits of the design constraints). An increase of the number of fingers can be achieved without increasing the size (or mass) of the rotor by decreasing the finger width. If however the fingers of the comb-drives are exceedingly slender, side pull-in of individual fingers can occur. The parameters that dominate this phenomenon are analyzed in the next section.

3. Side pull-in of individual comb fingers

It is assumed that the transverse stiffness of the suspension is sufficiently high to prevent transverse motion of the rotor. The present study aims to determine the limitations on the slenderness of the comb-drive fingers that ensure that side pull-in of individual fingers is also avoided. It is assumed that the extreme fingers on the sides of the rotor are each confined between two stator fingers (figure 1), and that the extreme fingers of the stator are sufficiently stiff such that their deformation is negligible.

A single rotor finger confined between two neighboring stator fingers is presented in figure 3. The rotor finger is of length L, width w and thickness b, and the gap g between the rotor and stator fingers is assumed to be uniform. A voltage difference V is applied between the rotor and stator, inducing the motion that determines the changing overlap $OL + x$. Assuming perfect symmetry, the rotor and stator fingers do not deform until the side pull-in instability develops.

The transverse equilibrium of a single finger is governed by

$$E^* I \frac{\mathrm{d}^4 y}{\mathrm{d}\xi^4} = \begin{cases} 0 & 0 \leqslant \xi \leqslant L - (OL + x) \\ \frac{1}{2}\varepsilon_0 b V^2 \left(\frac{1}{(g-y)^2} - \frac{1}{(g+y)^2}\right) & L - (OL + x) \leqslant \xi \leqslant L \end{cases} \tag{10}$$

where $E^* = E/(1 - \nu^2)$ is the effective elastic modulus in bending (assuming $b \gg w$), E and ν are the Young modulus and Poisson ratio of the structure material, respectively, $I = bw^3/12$ is the second moment of the beam cross-section, and ε_0 is the permittivity of free space. The effect of electrostatic fringing fields is ignored in the present analysis. For specific geometries, some simplified analytic approximations of the fringing field effect may be added to the model [9].

This governing equation may be rewritten in the following normalized form,

$$\frac{\mathrm{d}^4 \tilde{y}}{\mathrm{d}\tilde{\xi}^4} = \begin{cases} 0 & 0 \leqslant \tilde{\xi} \leqslant \alpha \\ \tilde{V}^2 \frac{\tilde{y}}{(1-\tilde{y}^2)^2} & \alpha \leqslant \tilde{\xi} \leqslant 1 \end{cases} \tag{11}$$

where

$$\tilde{\xi} = \frac{\xi}{L}, \qquad \tilde{y} = \frac{y}{g},$$
$$\Xi = \frac{OL + x}{L}, \qquad \alpha = 1 - \Xi, \tag{12}$$
$$\tilde{V}^2 = 24 \frac{\varepsilon_0 L^4}{E^* w^3 g^3} V^2.$$

The individual finger is clamped at its base and is assumed to be free of loads at its free edge ($\tilde{\xi} = 1$). Accordingly, the boundary conditions of the problem are

$$\text{at } \tilde{\xi} = 0: \qquad \tilde{y} = \tilde{y}' = 0 \tag{13a}$$

$$\text{at } \tilde{\xi} = 1: \qquad \tilde{y}'' = \tilde{y}''' = 0. \tag{13b}$$

At the verge of side pull-in of the individual finger, the deflection $\tilde{y}$ is small and therefore the distributed electrostatic force on the right-hand side of (11) may be approximated by the Taylor expansion

$$\tilde{V}^2 \frac{\tilde{y}}{(1 - \tilde{y}^2)^2} = \tilde{V}^2(\tilde{y} + 2\tilde{y}^3 + O(\tilde{y}^5)). \tag{14}$$

Omitting high-order terms, the governing equation reduces to

$$\frac{\mathrm{d}^4 \tilde{y}}{\mathrm{d}\tilde{\xi}^4} = \begin{cases} 0 & 0 \leqslant \tilde{\xi} \leqslant \alpha \\ \tilde{V}^2 \tilde{y} & \alpha \leqslant \tilde{\xi} \leqslant 1. \end{cases} \tag{15}$$

One solution of this equation is the trivial case of $\tilde{y} = 0$. In this case no bending occurs and the associated distributed mechanical forces (i.e. left-hand side of (15)) vanish as does the distributed electrostatic force (right-hand side of (15)). In the other solution, the distributed electrostatic forces are exactly balanced by the distributed mechanical restoring forces, for any arbitrary small deflection $\tilde{y}(\tilde{\xi})$. This means that for small deflections the stiffness of the system vanishes, and this is a bifurcation transition of the equilibrium state [10]. This bifurcation transition is related to the phenomenon of electromechanical buckling [11].

The nontrivial solution of (15) is given by

$$\tilde{y}_1 = b_0 + b_1\tilde{\xi} + b_2\tilde{\xi}^2 + b_3\tilde{\xi}^3 \qquad 0 \leqslant \tilde{\xi} \leqslant \alpha \tag{16}$$

$$\tilde{y}_2 = c_0\,\mathrm{e}^{-\lambda\tilde{\xi}} + c_1\,\mathrm{e}^{\lambda\tilde{\xi}} + c_2\sin(\lambda\tilde{\xi}) + c_3\cos(\lambda\tilde{\xi}) \quad \alpha \leqslant \tilde{\xi} \leqslant 1 \tag{17}$$

where b_0, b_1, b_2, b_3, c_0, c_1, c_2 and c_3 are constant parameters and the eigenvalue λ is given by

$$\lambda^4 = \tilde{V}^2. \tag{18}$$

From the clamping conditions (13a) we have

$$b_0 = b_1 = 0. \tag{19}$$

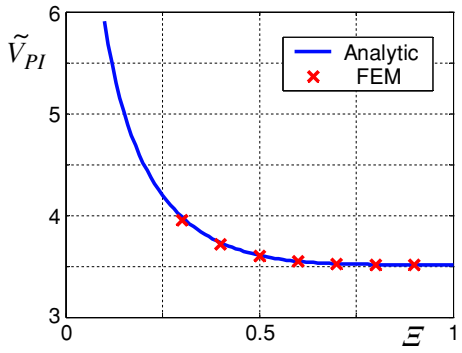

Figure 4. The normalized pull-in voltage as a function of the actual overlap.

The compatibility of the two domains requires that the deflection and its three derivatives be continuous at $\tilde{\xi} = \alpha$,

$$\begin{aligned} \tilde{y}_1(\alpha) &= \tilde{y}_2(\alpha) \\ \tilde{y}_1'(\alpha) &= \tilde{y}_2'(\alpha) \\ \tilde{y}_1''(\alpha) &= \tilde{y}_2''(\alpha) \\ \tilde{y}_1'''(\alpha) &= \tilde{y}_2'''(\alpha). \end{aligned} \tag{20}$$

Equations (20) and (13*b*) can be written in the following matrix form:

$$\begin{pmatrix} -\alpha^2 & -\alpha^3 & \mathrm{e}^{-\lambda\alpha} & \mathrm{e}^{\lambda\alpha} & \sin(\lambda\alpha) & \cos(\lambda\alpha) \\ -2\alpha & -3\alpha^2 & -\lambda\,\mathrm{e}^{-\lambda\alpha} & \lambda\,\mathrm{e}^{\lambda\alpha} & \lambda\cos(\lambda\alpha) & -\lambda\sin(\lambda\alpha) \\ -2 & -6\alpha & \lambda^2\,\mathrm{e}^{-\lambda\alpha} & \lambda^2\,\mathrm{e}^{\lambda\alpha} & -\lambda^2\sin(\lambda\alpha) & -\lambda^2\cos(\lambda\alpha) \\ 0 & -6 & -\lambda^3\,\mathrm{e}^{-\lambda\alpha} & \lambda^3\,\mathrm{e}^{\lambda\alpha} & -\lambda^3\cos(\lambda\alpha) & \lambda^3\sin(\lambda\alpha) \\ 0 & 0 & \lambda^2\,\mathrm{e}^{-\lambda} & \lambda^2\,\mathrm{e}^{\lambda} & -\lambda^2\sin(\lambda) & -\lambda^2\cos(\lambda) \\ 0 & 0 & -\lambda^3\,\mathrm{e}^{-\lambda} & \lambda^3\,\mathrm{e}^{\lambda} & -\lambda^3\cos(\lambda) & \lambda^3\sin(\lambda) \end{pmatrix} \times \begin{pmatrix} b_2 \\ b_2 \\ c_0 \\ c_1 \\ c_2 \\ c_3 \end{pmatrix} = \begin{pmatrix} 0 \\ 0 \\ 0 \\ 0 \\ 0 \\ 0 \end{pmatrix}. \tag{21}$$

The nontrivial solution is given by the first nonzero root of the determinant of the matrix. For the case of a complete overlap (i.e., $\alpha = 0$) only the marked part of the matrix in (21) is relevant. In this case the determinant results in the following transcendental equation which can be solved for the eigenvalue λ,

$$\cos(\lambda)\cosh(\lambda) + 1 = 0. \tag{22}$$

The first root of (22) is $\lambda_{\mathrm{I}} = 1.8751$. For increasing values of α, the determinant of the full matrix in (21) can be solved iteratively. The first root of this determinant $\lambda_{\mathrm{I}}(\alpha)$ is an increasing function of α. To ensure that the solution yields the first root $\lambda_{\mathrm{I}}(\alpha)$ for $\alpha > 0$, α is increased from $\alpha = 0$ in small increments and $\lambda_{\mathrm{I}}(\alpha_{i+1})$ is computed using the secant method beginning with the initial guess $\lambda_{\mathrm{I}}(\alpha_i)$ (with $\alpha_{i+1} > \alpha_i$).

Figure 4 illustrates the normalized side pull-in voltage as a function of the normalized overlap (solid line). For large overlaps, the voltage approaches the minimal value of $\tilde{V}_{\mathrm{PI}} = 3.516$.

In an actual electrostatic comb-drive, the driving voltage V is determined by the required travel range and the stiffness of the rotor suspension, as discussed in the previous section. Once the maximal value of the driving voltage has been determined in the design process, the minimal finger width w can be extracted from the definition of the normalized voltage, in the form:

$$w \geqslant \left(24\frac{\varepsilon_0 L^4}{E^* g^3}\frac{V_{\max}^2}{\tilde{V}_{\mathrm{PI}}^2}\right)^{\frac{1}{3}}. \tag{23}$$

If, as often is the case, the minimal feature and minimal trench are equal (i.e. $w = g$), then the minimal finger width w is given by

$$w \geqslant \left(24\frac{\varepsilon_0 L^4}{E^*}\frac{V_{\max}^2}{\tilde{V}_{\mathrm{PI}}^2}\right)^{\frac{1}{6}}. \tag{24}$$

For example, consider a single crystalline silicon (SCS) finger with $L = 150$ μm, $E = 130$ GPa, $\nu = 0.27$ and $\Xi = 0.9$, and assume that $w = g$. If the maximal driving voltage required to achieve the full travel range (i.e. $\Xi = 0.9$) is $V = 40$ V, then the minimal finger width is given by $w \geqslant 2$ μm.

4. Numerical validation

To validate the analytical result presented in the previous section, the electromechanical buckling problem is solved numerically using ANSYS8 finite element code with coupled-field analysis. A two-dimensional model of the problem is considered that accounts for electrostatic fringing field effects at the edges of the fingers (i.e. $\tilde{\xi} = \alpha$ and $\tilde{\xi} = 1$).

In reality, considerable fringing fields also occur at the edges of the fingers in the third dimension (i.e. $z = \pm b/2$), but this effect is not considered in this work. These fringing fields are strongly affected by specific geometrical parameters and some simple analytical approximations can be used to include them in the model [9].

The problem presented in figure 3 was modeled using square elements to model the rotor finger and the surrounding free space. The electromechanical critical buckling state was solved by using the DIPIE algorithm [12]. In the DIPIE algorithm the electromechanical problem in which instability occurs is solved by considering a series of equivalent problems, each of which is stable. According to this algorithm, the edge of the finger ($\tilde{\xi} = 1$, $\tilde{y} = 0$) is first subjected to an arbitrary transverse deflection $0 < \tilde{y} < 1$. This results in a transverse mechanical reactive force. Then, the voltage that eliminates this reactive force, while satisfying the static equilibrium of the electromechanical problem, is iteratively computed. This iterative computation converges rapidly because the equivalent electromechanical problem is stable (due to the fact that the finger edge is held at a fixed transverse deflection).

Figure 5 presents this voltage for different values of the enforced edge deflection. As shown, the maximal voltage is associated with the critical state, and the bifurcation is unstable [10].

The numerically computed electromechanical buckling voltage, as a function of the overlap, is presented in figure 4 ('$\times$' marks). The relative error between the analytic and numerical results is presented in figure 6 for various values of the actual overlap. As shown, the 2D in plane fringing field effect (at the finger tips) which is considered in the finite elements solution, is more pronounced for lower values of the actual overlap. Nevertheless, this effect is negligible, and the analytic and numeric results are in good agreement.

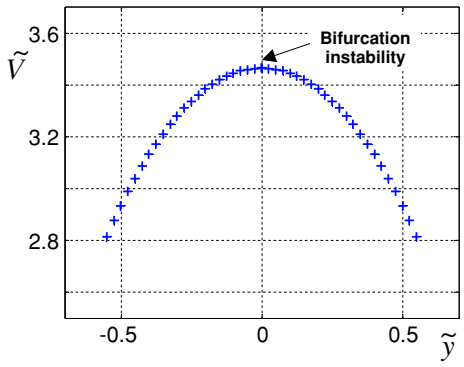

Figure 5. The normalized voltage that eliminates the reactive force as a function of the transverse deflection that is applied to the finger edge (for a typical geometry and an overlap of $\Xi = 0.9$).

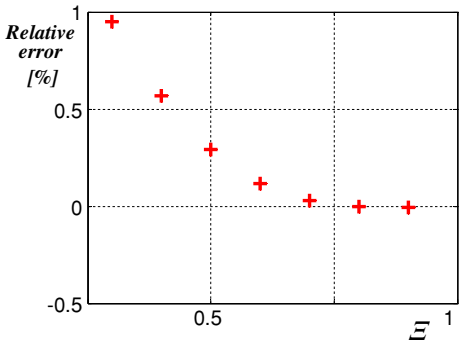

Figure 6. The relative error due to the 2D fringing fields (at the finger tips) between the analytic and FEM results as a function of the actual overlap.

5. Conclusion

In this work, the electromechanical stability of an individual comb-drive finger is considered. The critical state in which this stability is lost is solved analytically. It is shown that if the comb fingers are very slender, they may individually be affected by the side pull-in instability, even if side pull-in is prevented at the rotor level.

The analytic solution is in good agreement with finite element simulations. It is noted that the fringing fields in the third (out-of-plane) dimension are not considered in the analytic and numerical solutions. These fringing fields depend on specific geometrical parameters of the design (i.e. b/g) and can increase the electrostatic forces by a factor of up to 25% for typical cases [9]. Therefore, it is essential that this effect is considered in the design process, after the fabrication technology (and hence the device layer thickness b and the minimal trench size g) has been chosen.

When the comb-drive is part of a device that is subjected to accelerations or periodic loads, side pull-in instability of the rotor or of individual fingers may be expected to occur at lower voltages than predicted by the analysis presented in this work. This effect depends on the operation conditions of the device and should be considered accordingly.

Acknowledgment

This work was partially supported by *Intel Corporation*.

References

[1] Senturia S D 2001 *Microsystem Design* (Boston: Kluwer)
[2] Pelesko J A and Bernstein D H 2003 *Modeling MEMS and NEMS* (Boca Raton, FL: Chapman & Hall/CRC)
[3] Tang W C, Nguyen T C H and Howe R T 1989 Laterally driven polysilicon resonant microstructures *Sensors Actuators* **20** 25–32
[4] Legtenberg R, Groeneveld A W and Elwenspoek M 1996 Comb-drive actuators for large displacements *J. Micromech. Microeng.* **6** 320–9
[5] Elata D, Bochobza-Degani O and Nemirovsky Y 2003 Analytical approach and numerical alpha-lines method for pull-in hyper-surface extraction of electrostatic actuators with multiple uncoupled voltage sources *J. Microelectromech. Syst.* **12** 681–91
[6] Grade J D 1999 Large deflection, high speed, electrostatic actuators for optical switching applications *Mechanical Engineering* Stanford, p 232
[7] Grade J D, Jerman H and Kenny T W 2003 Design of large deflection electrostatic actuators *J. Microelectromech. Syst.* **12** 335–43
[8] Zhou G Y and Dowd P 2003 Tilted folded-beam suspension for extending the stable travel range of comb-drive actuators *J. Micromech. Microeng.* **13** 178–83
[9] Leus V and Elata D 2004 Fringing field effect in electrostatic actuators *Technical Report ETR 2004-2* Technion—Israel Institute of Technology
[10] Nguyen Q S 2000 *Stability and Nonlinear Solid Mechanics* (Chichester: Wiley)
[11] Abu-Salih S and Elata D 2004 The effect of internal stress on the electromechanical buckling of a clamped-clamped beam *European Micro and Nano Systems 2004 (Paris)*
[12] Bochobza-Degani O, Elata D and Nemirovsky Y 2002 An efficient DIPIE algorithm for CAD of electrostatically actuated MEMS devices *J. Microelectromech. Syst.* **11** 612–20